Transmission Line Fault Identification Using ANN and Time-Domain Measurements at Local Bus

تحديد أخطاء خطوط النقل باستخدام الشبكات العصبية الاصطناعية
و القياسات عند الطرف القريب فى نطاق الزمن

A. Elmitwally, Member, IEEE
Elect. Eng. Dept., Mansoura University,
Mansoura, 35516, Egypt

ملخص

يقدم البحث طريقتين لكشف و تشخيص أخطاء خطوط النقل الهوائية ذات الدائرة الواحدة، تعتمد أولاهما على استخدام عينات من موجات الجهد والتيار للأوجه الثلاث مقاسة عند جهة الإرسال تحت وجود الخطأ، بينما تعتمد الثانية على استخدام القيم الفعالة للجهد و التيار و تتميز أيضا بقدرتها على تحديد مكان الخطأ، و يتم تعديل الطريقة الثانية لتناسب الخطوط ذات الدائرتين بحيث يمكن تعيين دائرة الخطأ و كذلك نوعه، كما يقترح البحث أسلوبا مبتكرا لاكتشاف أخطاء الخطوط ذات الدائرة الواحدة التى تحدث خلال مقاومة كبيرة بمعالجة رقمية لإشارات تيارات الأوجه الثلاث المقاسة عند جهة الإرسال تستخدم إجراءات حسابية مبسطة، و كذلك تعديلا لهذا الأسلوب يخفض عدد عناصر مجموعة الصفات المميزة كما يجعله قادرا أيضا على تصنيف الخطأ بسرعة و دقة عاليين، والطرق المقدمة تبنى جميعها على استخدام شبكات عصبية اصطناعية ذات تصميم و تدريب مناسبين لاتخاذ القرار يعرضها البحث تفصيليا، وقد تم اختبار كل طريقة بعدد كاف من حالات الخطأ كما يتم مقارنة أداء الطرق المتنافسة.

Abstract: Among many applied techniques for overhead transmission line fault recognition, the artificial neural networks-aided schemes have demonstrated superior efficacy. This paper presents two methods based on time domain measurements at local end of the transmission line to identify the single circuit line fault type for low impedance faults. The first deals with time samples of the current and voltage waveforms of the three phases during the fault. The second uses the measured rms values of currents and voltages. The later can also determine the fault location on the line. It is also extended to produce the faulty circuit and fault type of double circuit lines for low impedance faults. Furthermore, the paper proposes a new algorithm for diagnosing the single line high impedance fault. A modified version of the algorithm is also developed to obtain a good representative feature vector with the least possible elements. The modification has enhanced diagnosing capabilities and can classify the high impedance faults. This enables the fast and accurate recognition of the faults that is a necessary request for the digital relaying system. The design and training of the decision making ANN for each approach are described. The studied techniques are tested with many cases to assess their diagnostic capabilities. Besides, the performance of the competitive methods is compared.

1. Introduction

Fast fault detection and equipment isolation is inevitable to maintain power system stability. Faults on transmission lines (TL) need to be detected rapidly, identified correctly and cleared in the shortest time. Transmission line fault detection module is essential to control other relaying modules [1-4]. The required detection technique should be adaptable to power system parameters and operating conditions variation. Conventional fault detectors require correct magnitudes of the current and voltage signals. When a fault occurs the power system goes into a transient period through which precise measurement of current and voltage is a tedious task [5-7].

Artificial neural networks is an apt pattern recognition tool that can distinguish between healthy and faulty states in a power system. Also, it is capable of discriminating the faulty phases (phase selection). ANN has many desired features like generalisation ability, noise rejection, robustness, high calculation speed, and error tolerance. Accordingly, decisions made by the ANN-based fault selector are not notably influenced by power system parameter variation or measurement noise [6-8]. Hence,

Accepted April 22, 2007

ANN-supported transmission line fault identification scheme is much advantageous.

In [2], a method is presented for TL fault detection and phase selection using ANN. The method uses current signals with zero and negative sequence currents to train an ANN. In [3], ANN is used to recognize the cause of fault in power distribution systems based on available field data collected for outages. In [6], a system is presented to locate faults on TL. Prony method is used to analyze the current and/or voltage signal at the local bus and extract its modal information. ANN is used to estimate the fault location based on the modal information. Different ANN structures are compared in [7] to search the best ANN structure for TL low impedance fault classification in single and double circuit transmission lines. Both pre-fault and post-fault current and voltage measurements are needed to construct the classifier.

ANN is applied to detect incipient high impedance fault (HIF) on power distribution feeders. The current samples used to train the ANN are separated into sets of one cycle interval. 20 mixed time and frequency domain parameters are taken to express each cycle in [8]. A numerical algorithm for arcing faults detection and locating is provided in [9]. It is based on the processing of time-domain local end currents and voltages signals. In [10], HIF detection method based on adaptive neuro-fuzzy inference system (ANFIS) is reported. The feature vector is obtained by dividing each current cycle into four windows and applying Fourier transform to each window. Other method for HIF detection is reported in [11] using wavelets and ANN. Most of the aforementioned approaches rely on lengthy and complex mathematical signal processing techniques to extract the feature vector. Some of them requires various currents and voltages measurements. This involves heavy computation burden and slows down the diagnosis process.

In this paper, three ANN-assisted schemes for identifying the single and double-circuit TL faults are presented. Time domain –based data processing of the local end measurements is used to get the dominant characteristics in each fault type. This is an imperative step to the precise identification of the fault and also its location on the line. Furthermore, the paper proposes new algorithms for detecting and diagnosing the single line HIF. Simplified methods for obtaining a good representative feature vector with the least possible elements are addressed. This enables the fast and accurate recognition of the faults at much reduced computational burden. The design and training of the decision making ANN that maps the feature vector space into the fault class and location spaces are described. The studied techniques are compared to assess their diagnostic capabilities.

2. Low Impedance Faults

2.1 Single circuit transmission line

Two approaches are used to identify faults of the single circuit TL. They are described in the following:

a) Using time samples of voltages and currents

The three-phase line to ground voltages and the three-phase currents of the faulted line are measured at the local end sampled at a frequency of 500 Hz. This results in 10 samples for each fundamental cycle. Five synchronised samples of each of the pointed out 6 waveforms are employed as the input vector discriminating the fault [1, 2]. They are combined sequentially in the order V_a, V_b, V_c, i_a, i_b and i_c. Thus forming a vector of 30 elements length (5 samples x 6 waveforms). This is the input vector introduced to the ANN classifier. Owing to a short time interval is involved in the input vector (half a cycle), the fault can be detected and categorized in about half a cycle that is fast enough for protection purposes.

400 fault situations were performed to the model power system of Fig.1 including 220 km, 220 kV TL for the different possible 10 fault

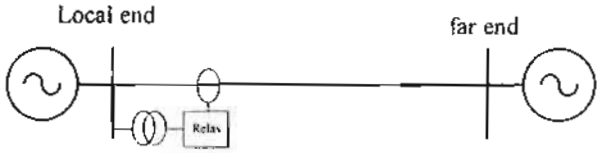

Fig.1 Model system with single circuit line

types formed by the A, B, C phases and the ground G (A-G, B-G, C-G, A-B, B-C, A-C, A-B-G, B-C-G, A-C-G, A-B-C-G). Different fault locations, fault incident angle and pre-fault conditions were assumed for each simulation case. Simulations were done using PSCAD/EMTDC software [12]. Fig.2 reveals the waveforms of two sample faults at 165km from the local end. The ANN classifier is designed and trained in the MATLAB environment [13, 14]. Its best structure is found to be composed of 4-layer feedforward neural network (FFNN) having one input layer of 30 neurons, two hidden layers of 35 and 20 neurons respectively, and an output layer of one neuron. The activation function of the hidden layers neurons are selected as hyperbolic tangent whereas that of the output layer is chosen to be linear [14]. The output of the classifier is a number from 1 to 10 referring to the fault class directly. The ANN classifier is trained with 400 training examples using a variety of competing algorithms as given in Table 1. The Levenberg-Marquardt (LM) training algorithm [14] is found to give the least training error of about 0.00000347 in 14 training epochs that is considered to be accurate enough. All the training examples are successfully recognised when approximating the ANN output to the

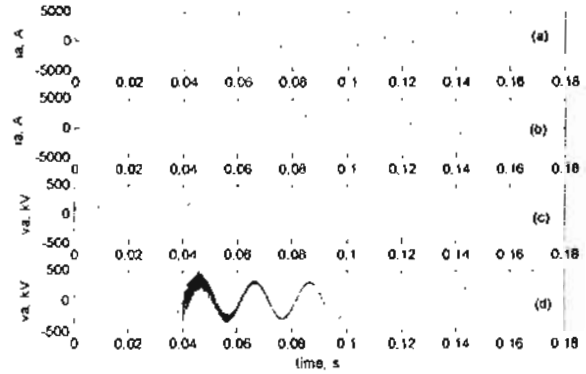

Fig. 2 Waveforms of two sample faults
(a), (c) current and voltage of phase a for A-G fault.
(b), (d) current and voltage of phase a for A-B fault.

nearest integer. The ANN classifier is tested with 20 different fault patterns and the classification efficiency was about 98%. Test results for a previously unseen 10 faults are given in Table 2.

b) Using rms values of voltages and currents

This method is based on measuring the rms values of the three phases voltages and flowing three phase currents at the local end of the line. The characterising vector consists of 6 elements (rms values). 2000 training examples are obtained by simulating the transmission system of Fig.1 in the PSCAD environment under different conditions such as fault type, fault location, fault incidence angle, and pre-fault current. The utilised ANN classifier is constructed in MATLAB. It is a 3 layer FFNN with 6 input neurons, 20 hidden neurons and 2 outputs. The first output is the fault type

Table 1. Performance of different training methods

Method	Levenberg-Marquardt	Gradient descent	Adaptive learning rate	Resilient back propagation	Fletcher conjugate gradient	Scaled conjugate gradient	One step secant	Polack conjugate gradient
Epochs	14	300	300	45	75	300	300	110
error	.00003	.2578	.0221	8.25	.0133	.00073	2.15	.01128

Table 2. Testing results for samples method

Fault type	A-G	B-G	C-G	A-B	A-C	B-C	A-B-G	A-C-G	B-C-G	A-B-C-G
ANN output	.998	1.99	2.998	3.99	5.001	6.0052	7	7.99	9.005	10.004
target	1	2	3	4	5	6	7	8	9	10

expressed in the decimal form (from 1 to 10) for the 10 known faults. The second is the distance at which the fault takes place measured from the local end of the line in km. The transfer function of the hidden neurons is hyperbolic tangent and that of the output layer is linear. The ANN is trained with the Levenberg-Marquardt (LM) method and has attained a training error of 0.0978 in 1000 training epochs[14]. This has been sufficient for the ANN to recognize the whole training set with 100% efficiency. Moreover, it has been able to identify 22 testing cases with accuracy 100% in detecting varying fault classes and its locations on the TL. It is worthy mentioning that no other training algorithms of the adopted ANN classifier has been able to give satisfactory performance. Table 3 shows the outcomes of testing the ANN for faults at 45 km from the local end. The provided excellent results assures the efficacy of this simple and light computational burden method.

the MATLAB/SIMULINK environment under different conditions such as faulty circuit, fault type, fault location, fault incidence angle, and pre-fault current [13]. The utilised ANN classifier is constructed in MATLAB. It is a 3 layer FFNN with 9 input neurons, 20 hidden neurons and 2 outputs. The first output is the fault type expressed in the decimal form (from 1 to 10) for the 10 known faults. The second is the faulty line assuming only one fault occurs at a time. The transfer function of the hidden neurons is hyperbolic tangent and that of the output layer is linear. The ANN is trained with the Levenberg- Marquardt method and has attained a training error of 0.098 in 1000 training epochs[14]. This has been sufficient for the ANN to recognize the whole training set with100% efficiency. Moreover, it has been able to identify 22 testing cases with accuracy 98% in detecting varying fault classes for both circuits.

Table 3. Testing results for rms method

Fault type	A-G		B-G		C-G		A-B		A-C		B-C		A-B-G		A-C-G		B-C-G		A-B-C-G	
ANN output	1	44.8	2	45.03	3	44.9	4	45.2	5	45.01	6	44.9	7	44.8	8	45.2	9	45.9	10	45.01
target	1	45	2	45	3	45	4	45	5	45	6	45	7	45	8	45	9	45	10	45

Table 4. Testing results for double circuit line

Fault type	A-G		B-G		C-G		A-B		A-C		B-C		A-B-G		A-C-G		B-C-G		A-B-C-G	
ANN output	98	1	2.03	1	2.98	1	4.01	1	5.03	1	5.68	1	7.11	1	8.15	1	9.02	1	9.98	1
target	1	1	2	1	3	1	4	1	5	1	6	1	7	1	8	1	9	1	10	1

2.2 Double circuit transmission line

A method is presented to identify the faulty circuit as well as the fault type in double circuit overhead transmission lines. The method is based on measuring the rms values of the three phases voltages at the local end and the flowing three phase currents for the two lines. This produces a characterising vector of 9 elements (rms values). 2000 training examples are obtained by simulating the 220kV, 200km double-circuit transmission system of Fig.3 in

Table 4 shows the outcomes of testing the ANN. The provided excellent results assures the efficacy of this light computational burden method compared to other techniques [1, 6].

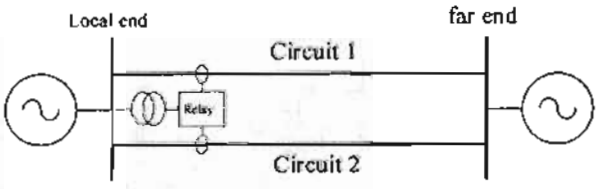

Fig.3 Model system with double circuit line

3. Detection of high impedance fault

3.1 The proposed algorithm

An ANN classifier is applied to discriminate faults occurring through high impedance in TL. It is a tedious task as the current and voltage waveforms are similar to their normal operation conditions for these types of faults. An adequate feature vector capable of portraying the fault characteristics is a key point to achieve the target. This vector is the input to the well-formed ANN classifier to detect the HIF. An algorithm is proposed in this paper to obtain an identifying feature vector as follows.

a) The instantaneous three-phase currents of the faulted line are measured at the local end sampled at a frequency of 500 Hz. This results in 10 samples for each fundamental cycle. 20 synchronised samples of each of the mentioned 3 waveforms (two fundamental cycles) are employed as the first part in the input vector discriminating the fault. They are combined sequentially in the order i_a, i_b and i_c forming a vector of 60 elements length (20 samples x 3 waveforms).

b)For each 20 samples in the former vector corresponding to (i_a, i_b and i_c, respectively) additional four values are estimated. The first is the mean square value that expresses the fault signal power. The second is the arithmetic mean value that represents the mean value of the decaying dc component characterising HIF current signals [6, 10]. The third is the maximum value that is the peak positive instantaneous fault current. The fourth is the minimum value that is the peak negative instantaneous fault current. This introduces another 12 elements (4 elements for each of the three phases).

c) The latter 12 elements are associated with the former 60 elements in the same order (a, b, and c) to give the overall input vector of 72 elements. This is the input vector introduced to the ANN classifier. However, the additional estimated 12 elements can be utilised alone to design an alternative ANN classifier scheme as described below in section 3.3.

3.2 Training the classifier

957 fault situations were performed to the model power system of Fig.1 for the different possible 10 fault types stated earlier. Different fault impedance, fault locations and pre-fault currents were assumed for each simulation case to obtain a sufficient training examples for the ANN classifier. A fault resistance of zero and 2000 ohms are considered as representatives to the low impedance fault (LIF) and the HIF conditions, respectively [6, 7]. This does not affect the generalization capability of the classifier as will be seen in the next sections. The adopted ANN classifier is able to detect faults on the TL taking place at different fault impedance values. Simulations were done using EMTDC/PSCAD software [12]. Fig.4 reveals the waveforms of two sample HIF faults at 165km from the local end and at 1000 ohms fault resistance.

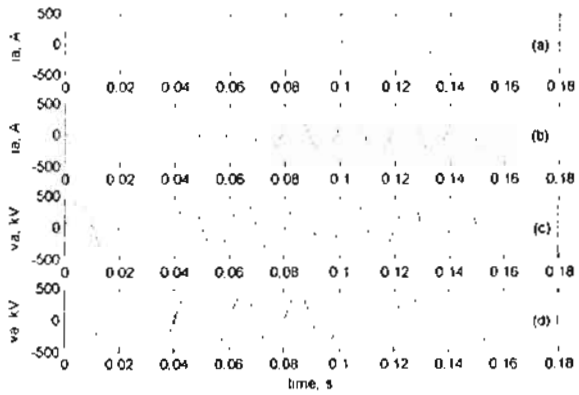

Fig. 4 Waveforms of two sample HIF faults
(a), (c) current and voltage of phase a for A-G fault.
(b), (d) current and voltage of phase a for A-B fault.

Three three-layer FFNNs ANN1, ANN2 and ANN3 are designed in the Matlab environment. ANN1 detects whether the fault is LIF or HIF for any fault resistance. It has 5 neurons in the hidden layer and 1 output neuron. ANN2 determines the fault location on the transmission line for the case of 2000 and zero ohms fault

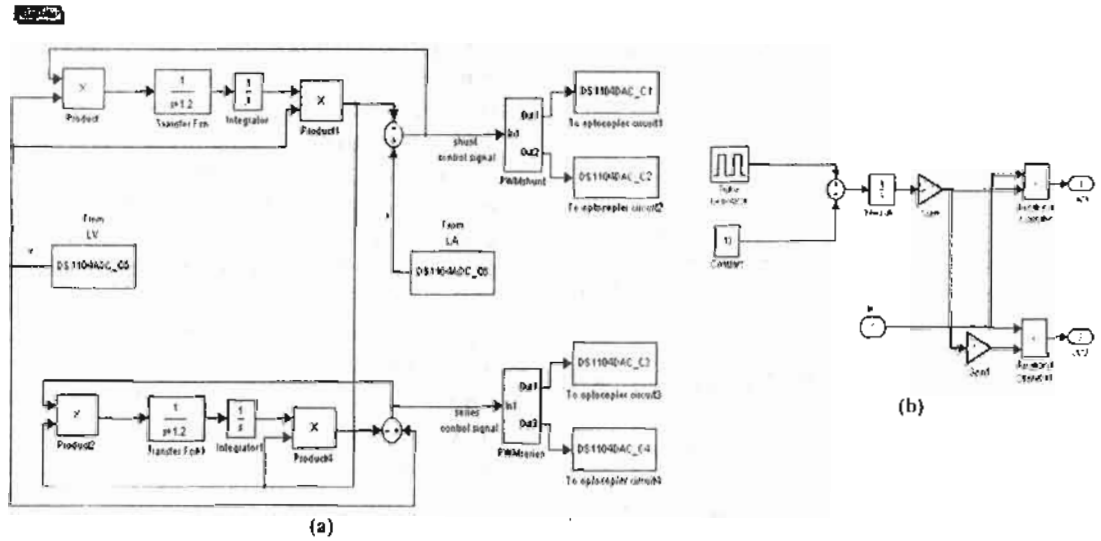

Fig. 5. (a) Control algorithm of a single phase UPFC and (b) PWM subsystem

The output of series converter is the input of series transformer (boosting transformer) which adds a series injected voltage to the mid-point voltage. Elements of the system are found in the Appendix.

5. PERFORMANCE OF UPFC

The UPFC is tested on laboratory for both shunt and series converters. The test results are shown in figures (6 – 15), and the values of all the quantities shown in these figures are given for two cases. Case 1 for light load and case 2 for heavy load.

Figures 6 and 7 show the phase relationships between the measured input voltage and the shunt converter control waveforms, and between the measured input current and the series converter control waveforms for cases 1 and 2, respectively.

Now, the converters' output is an important issue. In case 1, for light load of 244 mA, the measured input voltage is 204.4 V and leads line current by 72°. This phase shift is shown in fig. 6. The output voltage of the shunt converter has a 70 V (fixed) peak value and leads the input voltage by 90° as shown in Fig. 8. The value of shunt converter peak voltage can be controlled according to the required injected reactive current and this is left for the future work. In Fig. 9, the output voltage of the series converter leads the line current by 216° (or leads the measured voltage by 144°).

In case 2, for heavy load of 1.4 A, the waveforms of Fig. 10 show that the measured input voltage decreased to 153.3 V. The shunt converter output voltage is still leads the measured voltage by 90°. Figure 11 shows that the series converter output voltage leads the line current by 36°. Also, the magnitude of the series injected voltage can be adjusted by controlling the DC supply (link).

The output of each converter is injected to the mid-point of the simple power system throughout voltage transformer. Figures 12 and 13 show the voltage of point connecting the UPFC for cases 1 and 2, respectively. The voltage is increased to 219 volt for case 1 and reached 201 volt for case 2. Figures 14 and 15 show the mid-point voltage after adding the series injected voltage for both cases.

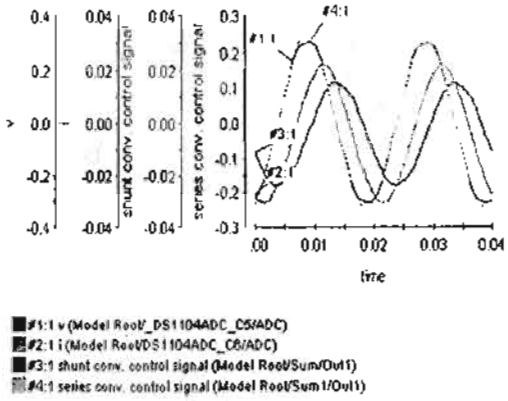

Fig. 6. Measured input voltage (v), input current (i), shunt converter control and series converter control waveforms for case (1)

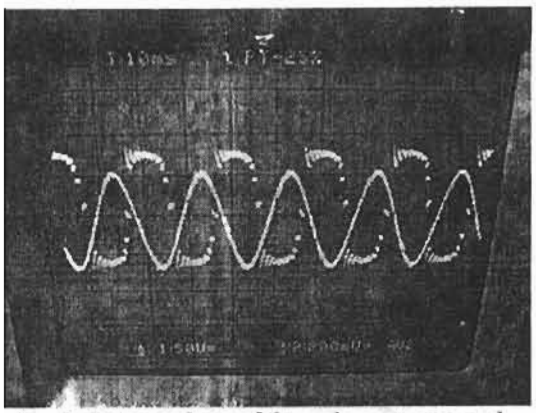

Fig. 9. Output voltage of the series converter and measured input current waveforms for case (1)

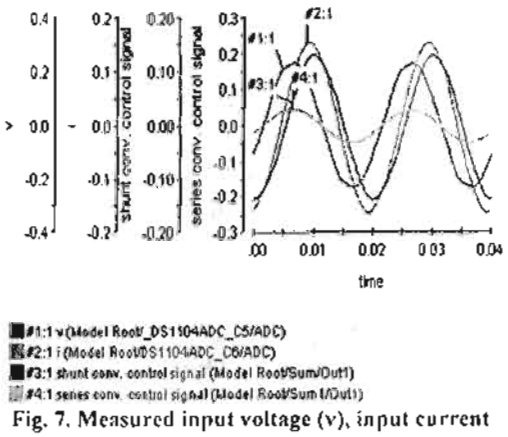

Fig. 7. Measured input voltage (v), input current (i), shunt converter control and series converter control waveforms for case (2)

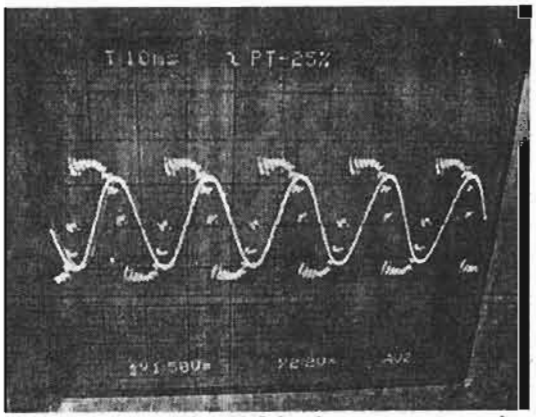

Fig. 10. Output voltage of the shunt converter and measured input voltage waveforms for case (2)

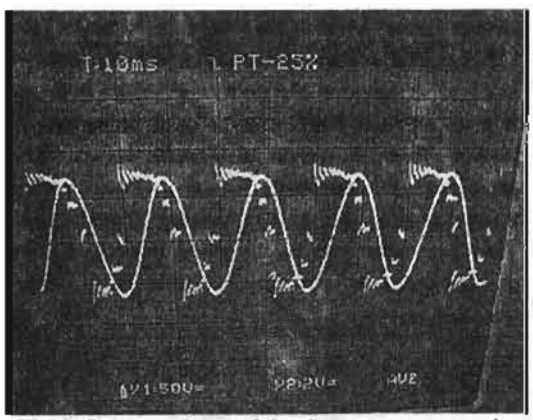

Fig. 8. Output voltage of the shunt converter and measured input voltage waveforms for case (1)

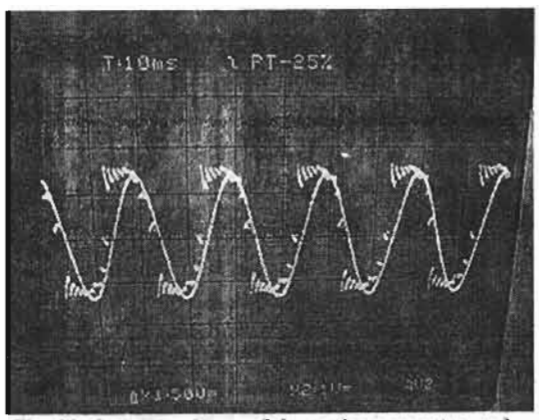

Fig. 11. Output voltage of the series converter and measured input current waveforms for case (2)

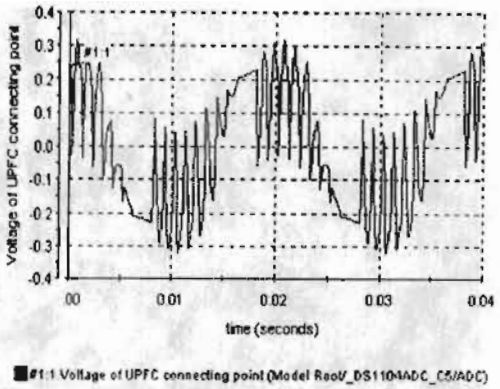

Fig. 12. UPFC connecting point voltage waveform for case (1)

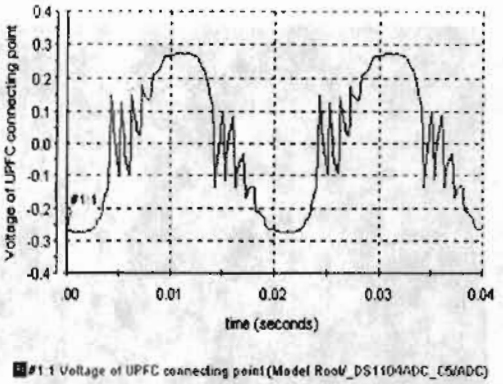

Fig. 13. UPFC connecting point voltage waveform for case (2)

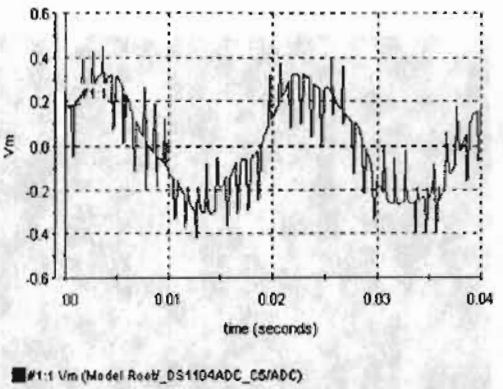

Fig. 14. Boosted mid-point voltage waveform for case (1)

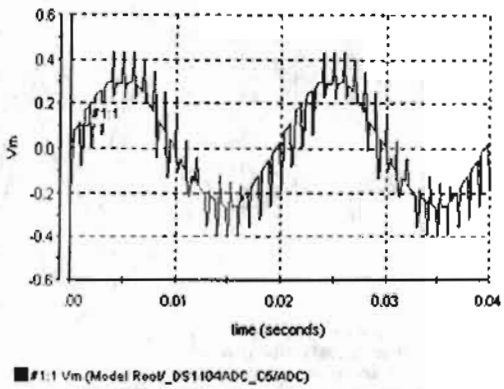

Fig. 15. Boosted mid-point voltage waveform for case (2)

6. CONCLUSION

Digital signal processor (DSP) – based single phase unified power flow controller (UPFC) has been implemented. A simple and efficient UPFC control algorithm has been achieved for both shunt side and series side. This algorithm is based on the active power filter current reference calculation method. The PWM voltage source converters linked by DC source have been taken as an UPFC. The experimental results have been analyzed. The shunt converter output voltage is found in quadrature with the bus voltage connecting UPFC and achieves voltage support. The series converter output voltage leads line current by an angle dependent on the required power flow in the line which includes the UPFC. The effect of series converter control is clear in large scale power systems because it can control the amount and direction of power flow between different buses. The problem of harmonics found in the injected waveforms is due to the voltage transformer. This problem can be avoided practically by using suitably designed shunt and series transformers.

7. APPENDIX

The elements used in laboratory are:
PC Host, Windows98, Matlab6.1(R12.1)/ Simulink, DSP-TMS320C31 Hardware, DSpaceR4.3 Software, 2 Single-Phase 250 Km T.L. model, Single-Phase source (220 volt, 50 Hz), 2 Single-Phase 400 Watt / 300 Var variable (R-L) load, 1 LV25-P (400 V), 1 LA25-NP (25 A), Optoisolator circuit (4N35), Two H-bridges each consists of 4-power MOSFETs (IRFP460), Fixed 70 volt DC supply and single phase voltage transformer 220/57.7 volt.

8. REFERENCES

[1] L. Gyugyi et al., "The Unified Power Flow Controller: A New Approach To Power Transmission Control," IEEE Trans. On Power Delivery, Vol. 10, No. 2, pp. 1085-1097, April 1995.

[2] C. D. Schauder et al., "Operation of the Unified Power Flow Controller Under Practical Constraints," IEEE Trans. Power Delivery, vol. 13, No. 2, pp. 630–639, Apr. 1998.

[3] Kalyan K. Sen and Eric J. Stacey, "UPFC – Unified Power Flow Controller: Theory, Modeling, and Applications," IEEE Trans. Power Delivery, vol. 13, No. 4, pp. 1453–1460, October 1998

[4] H. A. Abdelsalam, M. Abdelkrim, G. E. M. Aly, and K. M. Shebl, "Using UPFC for Power Flow Control and Dynamic Stability," Tenth International Middle-East Power Systems Conference (MEPCON'2005) Dec. 13-15, 2005, Port Fouad, Port Said, Egypt.

[5] S. Mobin, E. Hiraki, H. Takano and M. Nakaoka, "Simulation Method for DSP-Controlled Active PFC High-Frequency Power Converters," IEE Proc.-Electr. Power Appl., vol. 147, No. 3, pp. 159–165, May 2000.

[6] B. N. Singh, A. Chandra and K. Al-Hadad, "DSP-Based Indirect Current Controlled STATCOM Part 1: Evaluation of Current Control Techniques," IEE Proc.-Electr. Power Appl., vol. 147, No. 2, pp. 107–112, March 2000.

[7] B. N. Singh, A. Chandra and K. Al-Hadad, "DSP-Based Indirect Current Controlled STATCOM Part 2: Multifunctional Capabilities," IEE Proc.-Electr. Power Appl., vol. 147, No. 2, pp. 113–118, March 2000.

[8] M. E. Abdel-Karim and A. I. Taalab, "A Single Phase Series Active Power Filter for Harmonic Compensation of Nonlinear Loads," Engineering Research Bulletin, Menoufiya University, Faculty of Engineering, Shebine El-Kom, Egypt, vol. 19, No. 3, pp 73-86, Sept.-Oct. 1996.

[9] M. Abdel-Karim, "Reactive and harmonic current detection in a nonlinear load with frequency excursions," Alexandria Engineering Journal, Faculty of Engineering, Alexandria University, Egypt, vol. 41, No. 3, pp 423-432, May 2002.

[10] B. R. Lin , D. J. Chen, "Single-Phase Neutral Point Clamped AC/DC Converter with the Function of Power Factor Corrector and Active Filter," IEE Proc.-Electr. Power Appl., vol. 149, No. 1, January 2002.